Int. J. Multiphase Flow Vol. 14, No. 4, pp. 439–458, 1988
Printed in Great Britain.

0301-9322/88 $3.00 + 0.00

PHASE SEPARATION IN DIVIDING TWO-PHASE FLOWS

S. T. HWANG,† H. M. SOLIMAN‡ and R. T. LAHEY JR
Department of Nuclear Engineering and Engineering Physics, Rensselaer Polytechnic Institute, Troy, NY 12180-3590, U.S.A.

(*Received* 2 *March* 1987; *in revised form* 22 *January* 1988)

Abstract—Phase separation in dividing T- and Y-junctions was investigated experimentally and analytically in this study. New air/water phase separation data are presented for three horizontal test sections (a T-junction, a 45° Y-junction and a 135° Y-junction). Emphasis was placed on low extraction rates through the side branch. A phenomenological model was developed which was based on the idea of dividing streamlines in which centrifugal and interfacial drag forces were assumed to be dominant. Comparisons between model predictions and the available data, corresponding to different flow regimes, pressures, fluid properties, inlet flow rates and qualities and extraction rates, showed good agreement thus supporting the assumptions inherent in the model.

Key Words: phase separation, two-phase flow

1. INTRODUCTION

Two-phase flow in branching conduits occurs in many industrial applications such as nuclear reactors, chemical process plants and in the petroleum industry. Phase separation in branching conduits can have a profound effect on system performance. Examples include: the effect of phase separation in the main coolant piping on the effectiveness of core cooling for a light-water nuclear reactor (LWR) during a hypothetical loss-of-coolant-accident (LOCA); the effectiveness of wet steam injection systems for enhanced oil recovery; and the design of (liquid) slug catchers and phase separators for off-shore oil well platforms.

Let us first consider the lessons learned to date from experimental data and the analysis of the observed phenomena. Collier (1975) presented the data of St Pierre, which were taken in a horizontal T-junction in which the diameter of the inlet pipe and run was 0.038 m, while that of the branch was 0.025 m. These data showed that over a wide range of mass extraction rates (w_3/w_1) almost complete phase separation occurred (i.e. $x_3/x_1 = [w_3/w_1]^{-1}$). These trends seem reasonable since the vapor phase normally has far less inertia than the liquid phase (i.e. $\rho_G u_G^2 \ll \rho_L u_L^2$), thus the vapor can be expected to more easily turn the corner into the side branch.

Honan & Lahey (1981) ran air/water phase separation experiments in vertical 0.038 m dia Plexiglas Y- and T-junction test sections for bubbly and churn/turbulent flows. Their data also showed that almost complete phase separation occurred and that the phase separation ratio (x_3/x_1) is strongly affected by the flow split (w_2/w_3). Indeed, they found that, for the conditions tested, the mass extraction rate (w_3/w_1) had much more effect on phase separation than the separation angle (θ) between the branch and the run, and the inlet mass flux (G_1).

Zetzmann (1982) presented similar data for low-pressure ($p < 0.3$ MPa) air/water two-phase flows using T- and 45° Y-junction test sections in vertical and horizontal configurations. He only performed experiments for a narrow range of mass extraction rates for the T-junction test section, however, data were taken over a wider range for the Y-junction test section.

Azzopardi & Whalley (1982) took annular flow data in T-junctions for horizontal and vertical orientations. They also found that the phase separation phenomena was strongly effected by the mass withdrawal rate (w_3/w_1), flow regime, operating conditions and test section geometry and orientation. Reimann & Seeger (1983) took data for stratified horizontal flows. Again, they found that phase separation depended strongly on the mass extraction rate, flow regime and test section geometry (i.e. the orientation of the simulated small break).

†‡Current addresses: †Fuel Engineering Department, Combustion Engineering Inc., 1000 Prospect Hill Rd, Windsor, CT 06095, U.S.A.; and ‡Department of Mechanical Engineering, University of Manitoba, Winnipeg, Manitoba R3T 2N2, Canada.

To date, several researchers have tried to develop models for the prediction of phase separation in branching conduits. Zetzmann (1982) used the fact that the parameters which most strongly affected phase separation were the mass extraction rate (w_3/w_1), the diameter ratio (D_3/D_1), the inlet mass flux (G_1) and the angle (θ) between the branch and run. He developed an empirical correlation based on his data. Unfortunately, his data base was limited and thus his correlation is of limited practical value.

Henry (1981), who took phase separation data in a horizontal T-junction, also proposed an empirical correlation. Again, this correlation is only valid in a limited range of hydraulic conditions.

Seeger (1985) took phase separation data in a T-junction for both air/water and steam/water flows. His steam/water data deserve special attention, since they represent high-pressure conditions. Significantly, the observed phase separation was similar to that in air/water flows. Thus, flashing does not appear to have a significant influence on phase separation. Unfortunately Seeger did not propose a mechanistic phase separation model. Rather, he also proposed an empirical correlation which is presumably only valid over a limited range of conditions.

Saba & Lahey (1984) proposed a mechanistic model which was based on the concept of dividing streamlines. Unfortunately this model is only valid for the higher mass extraction rates (i.e. $w_3/w_1 \geqslant 0.3$), where a fairly large portion of gas arriving at the junction is extracted through the side branch.

Azzopardi & Whalley (1982) and Azzopardi & Baker (1981) developed phenomenologically-based models for low mass extraction rates (i.e. $w_3/w_1 < 0.1$) for annular and bubbly/churn flows, respectively. They defined a "zone of influence" from which each phase was extracted through the branch. Unfortunately, their models are only applicable over a limited range of interest.

In the study presented herein new experimental data on phase separation in horizontal Y- and T-junctions are reported. Special emphasis was given to low mass extraction rates (i.e. $w_3/w_1 < 0.3$), since very little data existed for these conditions. It should be noted that Honan & Lahey (1981) and Zetzmann (1982) investigated dividing two-phase flows in test sections having a vertical orientation; while Saba & Lahey (1984), and the new data discussed herein, were taken in a horizontal configuration. It was found that test section orientation is not significant in many cases of interest, however, the location of the side branch can have a significant effect for horizontal conduits (Smoglie *et al.* 1986).

2. EXPERIMENTAL CONSIDERATIONS

From the data and insight gained from previous research we know that pronounced phase separation can occur in branching conduits and that the degree of phase separation is strongly dependent on the flow split (w_2/w_3), conduit geometry (e.g. D_3/D_1) fluid properties ($\rho_L, \rho_G, \ldots$) and the flow regime at the inlet of the junction. However, prior to this study very little emphasis was placed on the low extraction rate region for flow regimes other than annular flow.

The air/water test loop used in this program is shown in figure 1. It consisted of a branching test section, open air and closed water loops, and the related instrumentation and computer data acquisition system.

The test sections (i.e. the T- and Y-junctions) were made from Plexiglas and each branch had the same dimensions (i.e. $D_1 = D_2 = D_3 = 0.038$ m i.d.). There were numerous static pressure taps along the test section which provided detailed information on the pressure distribution along the test section (especially in the region of the junction). Also, to assure fully-developed flow, additional copper piping having the same inside diameter as the test section was installed in all branches. To determine the flow quality at the exit from the branch and run, the mass flow rate of each phase was separately measured using orifices or rotameters after the air/water mixture was separated in special separator tanks. Having these flow rates, the flow quality at section i is given by

$$x_i = \frac{w_{G_i}}{w_{G_i} + w_{L_i}} \quad (i = 1, 2, 3).$$

To assess the accuracy of these data we applied the continuity equation for both phases and rejected any data which did not satisfy continuity within $\pm 5\%$.

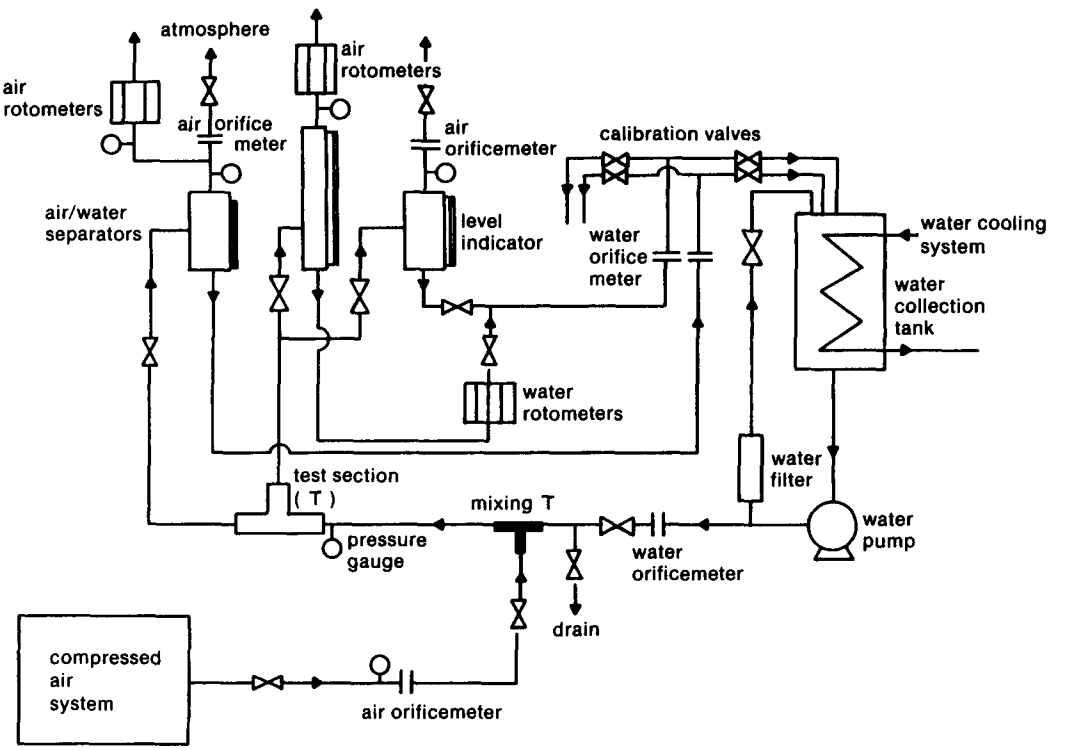

Figure 1. Air/water loop.

3. EXPERIMENTAL RESULTS

Phase separation experiments for dividing flows were performed for the horizontal test section configurations shown in figure 2 and the following operating conditions:

Mass fluxes
(1) low mass flux: $G_1 \cong 1350$ (kg/m^2 s)
(2) medium mass flux: $G_1 \cong 2050$ (kg/m^2 s)
(3) high mass flux: $G_1 \cong 2700$ (kg/m^2 s).

Inlet qualities
$x_1 = 0.2$, 0.3 and 0.4%.

Mass extraction ratios (w_3/w_1)
$\sim 0.02 \leqslant w_3/w_1 \leqslant \sim 0.95$.

High-speed still photography was also performed to provide enhanced visualization of the flow at and around the junction.

It was found that when $w_3/w_1 > 0.3$, virtually complete phase separation took place. For example, as can be seen in figure 3, nearly complete phase separation occurs at $w_3/w_1 = 0.31$. Moreover, due to the adverse pressure gradient in the run, we observe that some portion of the gas phase returned to the side branch after passing through the junction to the run. Similar behavior was noted in the 45° Y-junction, as can be seen in figure 4. Figure 5 shows essentially complete phase separation at $w_3/w_1 \cong 0.52$ for the 135° Y-junction.

Let us now consider the observed trends in the phase separation data taken in this study. These trends can be seen in figure 6. We note that for large extraction rates (w_3/w_1) essentially complete phase separation [i.e. $x_3/x_1 = (w_3/w_1)^{-1}$] occurs no matter what the angle (θ) of the side branch is. In contrast, for intermediate extraction rates there is a peak in x_3/x_1 and the degree of phase separation depends on θ. Moreover, it can be noted that for low extraction rates there are values of $x_3/x_1 < 1$ and the data trends indicate $x_3/x_1 \to 0$ as $w_3/w_1 \to 0$.

These data trends make sense if we recall that the liquid phase normally has more axial inertia than the vapor phase and thus it is harder for it to change direction and exit through the side branch than the gas phase. This is particularly true for large θ. Moreover, the data trends for low extraction

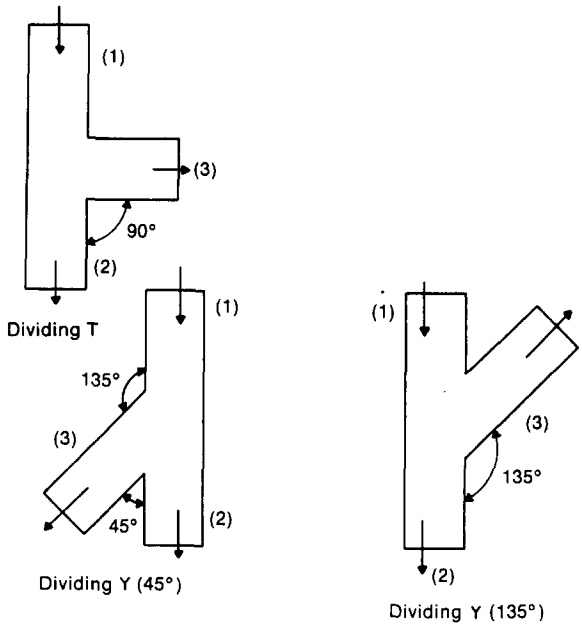

Figure 2. Test sections and flow configurations.

rates are consistent with a "zone of influence" which is close to the side branch opening. In this region the axial inertia of the liquid phase is relatively low and the concentration of vapor may also be low. Thus we may have $x_3/x_1 < 1$.

4. ANALYTICAL MODELING

4.1. Introduction

In the analysis of phase separation in branching conduits there are numerous variables, however, for steady-state conditions they can be categorized as: the three flow rates, w_i, and flow qualities,

Figure 3. Phase separation—dividing T-junction (top view). $w_1 = 2.284$ (kg/s), $x_1 = 0.2106$ (%), $w_3/w_1 = 0.3108$, $x_3/x_1 = 2.608$, $p_1 = 0.1484$ (MPa).

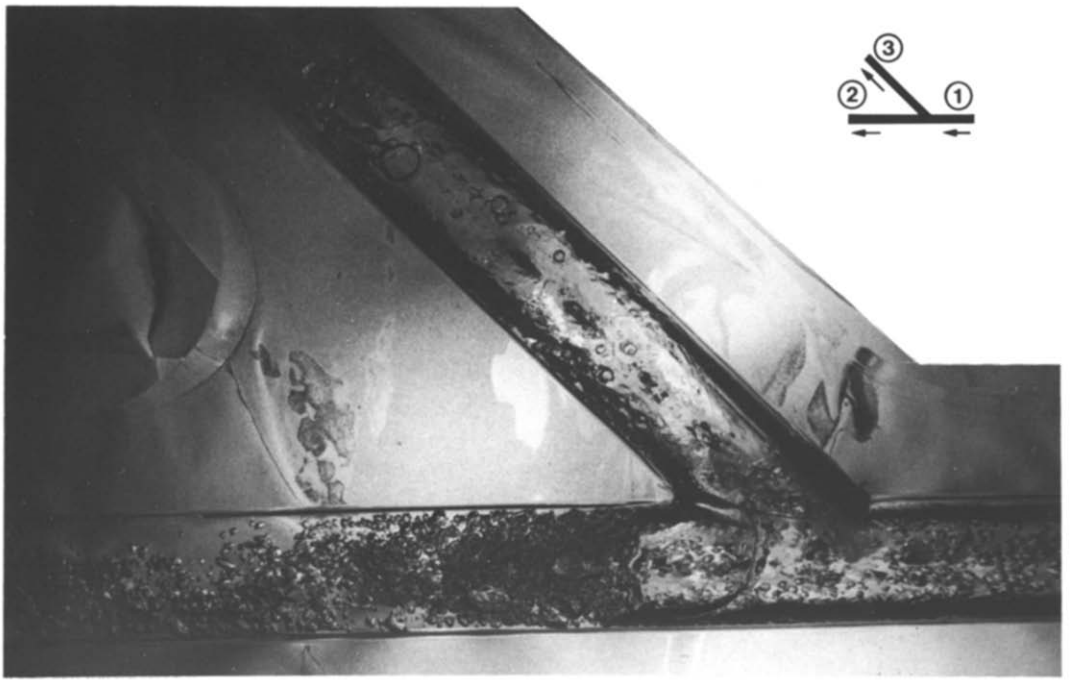

Figure 4. Phase separation—dividing Y-junction (45°, top view). $w_1 = 1.600$ (kg/s), $x_1 = 0.1964$ (%), $w_3/w_1 = 0.2105$, $x_3/x_1 = 4.186$, $p_1 = 0.1422$ (MPa).

x_i, and the pressure drops, Δp_{13_j} and Δp_{12_j}. This gives a total of eight variables. Of the eight, we normally specify three of these variables (e.g. w_1, x_1 and w_3; or x_1, Δp_{13_j} and Δp_{12_j} etc.). We must then have relationships for the remaining five variables. Four of the equations which are needed to calculate phase separation in branching conduits are:

the steady-state continuity equations,

$$w_1 = w_2 + w_3 \qquad \text{(mixture)}, \qquad [1]$$

$$w_1 x_1 = w_2 x_2 + w_3 x_3 \qquad \text{(vapor phase)}; \qquad [2]$$

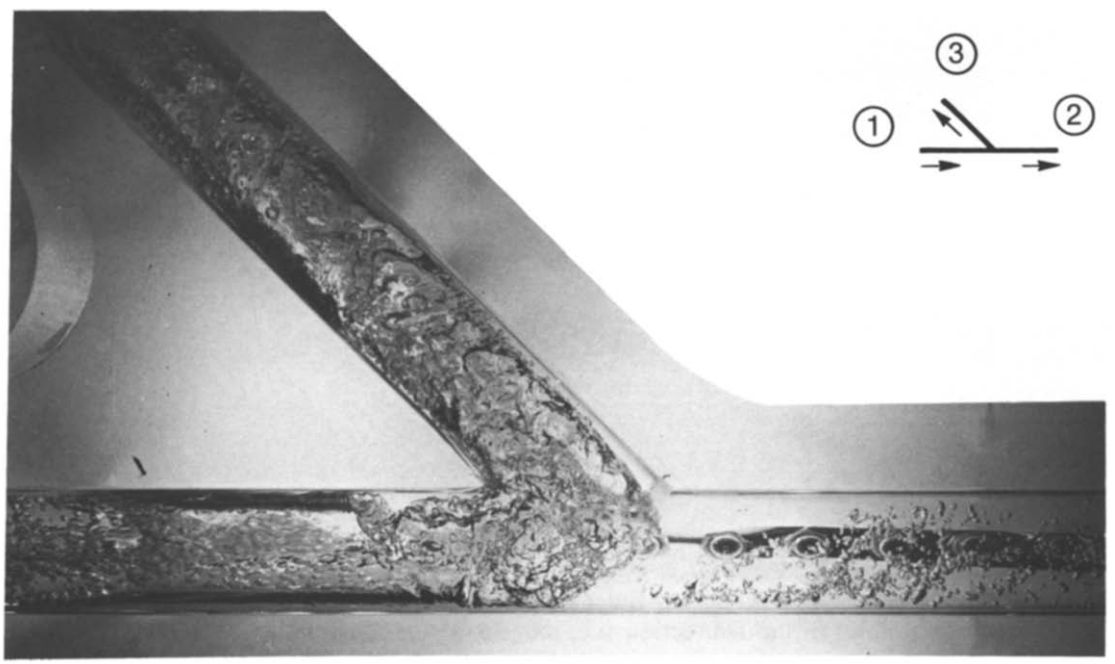

Figure 5. Phase separation—dividing Y-junction (135°, top view). $w_1 = 1.579$ (kg/s), $x_1 = 0.2001$ (%), $w_3/w_1 = 0.5172$, $x_3/w_1 = 1.810$, $p_1 = 0.1359$ (MPa).

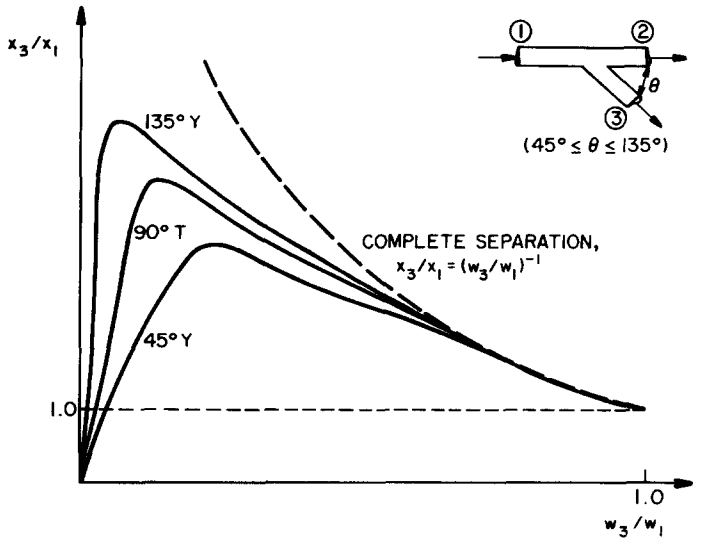

Figure 6. Phase separation trends in dividing Y- and T-junctions.

and

the steady-state mixture momentum equations,

$$\Delta p_{13} = \Delta p_{1-1_J} + (\Delta p_{13})_J + \Delta p_{3_J-3}, \quad \text{(branch)} \tag{3}$$

$$\Delta p_{12} = \Delta p_{1-1_J} + (\Delta p_{12})_J + \Delta p_{2_J-2} \quad \text{(run);} \tag{4}$$

where the static pressure change in the inlet and outlet branches is given by

$$\Delta p_{i-1_J} = \Delta p_{i_J-1} = K_i \frac{G_i^2}{2\rho_L} \phi_{L0_i}^2 + \bar{\rho}_i g L_i \sin\theta_i \quad (i = 1, 2, 3) \tag{5}$$

and

$$K_i = f_i \frac{L_i}{D_H}.$$

The static pressure change in the junction is given by

$$(\Delta p_{13})_J = \frac{\langle \rho_{H_3} \rangle}{2} \left(\frac{G_3^2}{\langle \rho_3''' \rangle^2} - \frac{G_1^2}{\langle \rho_1''' \rangle^2} \right) + \frac{G_1^2}{2\rho_L} K_{13} \Phi_{13} \tag{6}$$

and

$$(\Delta p_{12})_J = \frac{K_{12}}{2} \left(\frac{G_2^2}{\langle \rho'_2 \rangle} - \frac{G_1^2}{\langle \rho'_1 \rangle} \right). \tag{7}$$

The details of these pressure drop equations have been reported elsewhere (Lahey 1986; Hwang & Lahey 1988) and thus will not be repeated herein. Let us now consider the specification of the remaining (fifth) equation.

4.2. The Analysis of Phase Separation in a Dividing T-junction

4.2.1. Background

Let us postulate the existence of mean "streamlines" for each phase, such as that shown in figure 7. We can employ a modified version of Euler's equations of motion for a fluid particle travelling on a curved streamline. In the s-direction (i.e. tangent to the streamline), we have

$$\frac{\partial p}{\partial s} = -\rho_k u_k \frac{\partial u_k}{\partial s} + F_{D_{k,s}}, \tag{8}$$

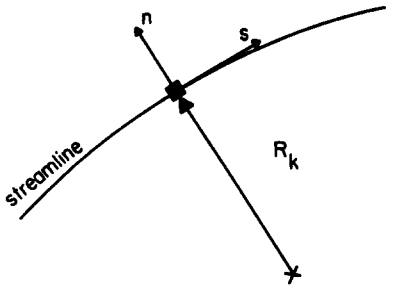

Figure 7. A typical streamline.

where u_k is the velocity of phase k along the streamline and $F_{D_{k,s}}$ is the component of the interfacial drag force per unit volume in the s-direction. In the normal (n)-direction, we have

$$\frac{\partial p}{\partial n} = \rho_k \frac{u_k^2}{R_k} + F_{D_{k,n}}, \qquad [9]$$

where R_k is the radius of curvature of the streamline for phase k and $F_{D_{k,n}}$ is the component of the interfacial drag force per unit volume in the direction normal to the streamline.

4.2.2. Proposed approach

In the region of the junction the flow situation is very complicated and exact analysis is difficult if not impossible. Nevertheless, a simplified phenomenological approach can be used. As shown in figure 8, this approach is based on the idea that the gas and liquid flows going into the side branch are coming from regions (i.e. "zones of influence") bounded by dividing streamlines. The initial positions of these streamlines in the inlet branch are given by δ_L and δ_G, respectively, for the liquid and gas phase. For a given geometry (D_1 and D_3), fluid properties ($\rho_G, \rho_L, \ldots$) and inlet flow conditions ($w_1, x_1, \ldots$) a method for calculating δ_G for a given δ_L, or vice versa, must be developed.

Whether the gas flows into the side branch or not, depends on the balance of forces on each phase. Figure 9 shows the relevant forces acting on the gas and liquid at a typical streamline crossing. This figure indicates that the two streamlines cross at an angle β. The gas and liquid velocities along these streamlines are $\mathbf{u}_G$ and $\mathbf{u}_L$, respectively. Due to phasic slip, a volumetric drag force, F_{D_G}, acts on the gas and an equal and opposite drag force, $F_{D_L} = -F_{D_G}$, acts on the liquid. Both drag forces act in a direction parallel to the relative velocity ($\mathbf{u}_G - \mathbf{u}_L$) vector. Due to the motion along curved streamlines, the centrifugal forces per unit volume, $\rho_G u_G^2/R_G$ and $\rho_L u_L^2/R_L$, act on the gas and liquid phase, respectively, in directions normal to their streamlines.

Applying the modified Euler s and n equations to the gas phase yields

$$\frac{\partial p}{\partial s_G} = -F_{D_G} \sin\gamma - \rho_G u_G \frac{\partial u_G}{\partial s_G} \qquad [10]$$

and

$$\frac{\partial p}{\partial n_G} = F_{D_G} \cos\gamma + \rho_G \frac{u_G^2}{R_G}. \qquad [11]$$

Similarly, for the liquid phase,

$$\frac{\partial p}{\partial s_L} = F_{D_L} \sin(\gamma - \beta) - \rho_L u_L \frac{\partial u_L}{\partial s_L} \qquad [12]$$

and

$$\frac{\partial p}{\partial n_L} = -F_{D_L} \cos(\gamma - \beta) + \rho_L \frac{u_L^2}{R_L}. \qquad [13]$$

Dynamic equilibrium exists when the resultant volumetric forces acting on the gas and the liquid are equal in magnitude and direction. This condition is shown graphically in figure 10 in which,

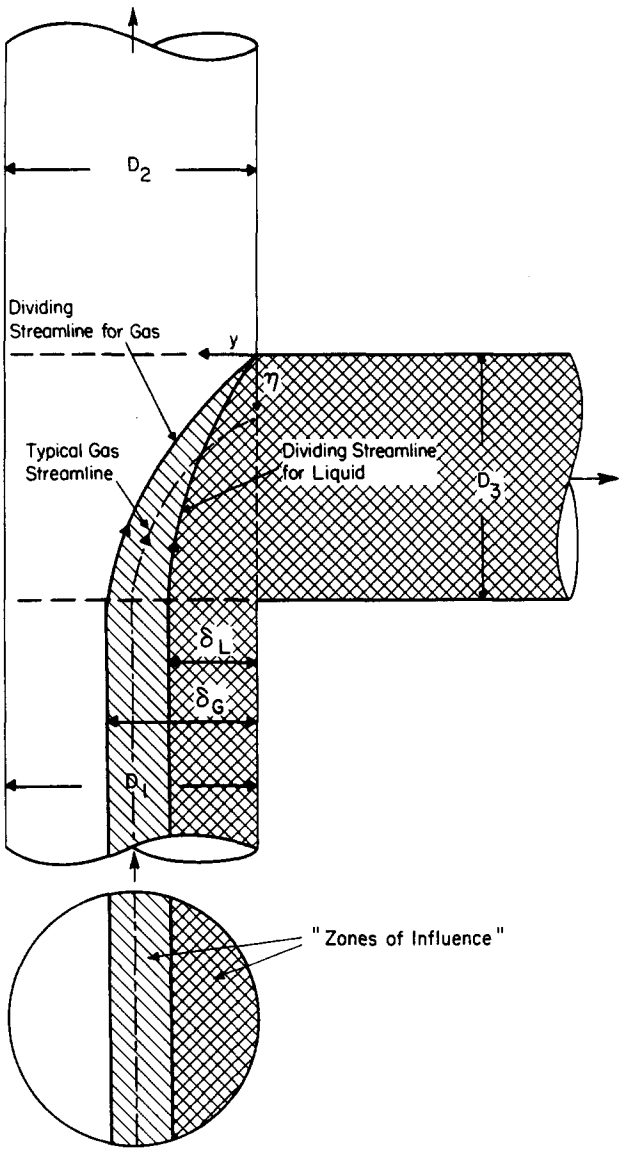

Figure 8. Phase separation model based on dividing streamlines.

for simplicity, we have neglected spatial acceleration and the individual forces in [10]–[13] are identified.

If we denote $F_D \triangleq |F_{D_L}| = |F_{D_G}|$, then the equilibrium condition is easily deduced from figure 10 as

$$2F_D \sin\gamma = \frac{\rho_L u_L^2}{R_L} \sin\beta \qquad [14]$$

and

$$2F_D \cos\gamma = \frac{\rho_L u_L^2}{R_L} \cos\beta - \frac{\rho_G u_G^2}{R_G}. \qquad [15]$$

Dividing [14] by [15], we obtain

$$\tan\gamma = \frac{\sin\beta}{\left[\cos\beta - \left(\frac{\rho_G}{\rho_L}\right)\left(\frac{u_G}{u_L}\right)^2\left(\frac{R_L}{R_G}\right)\right]}. \qquad [16]$$

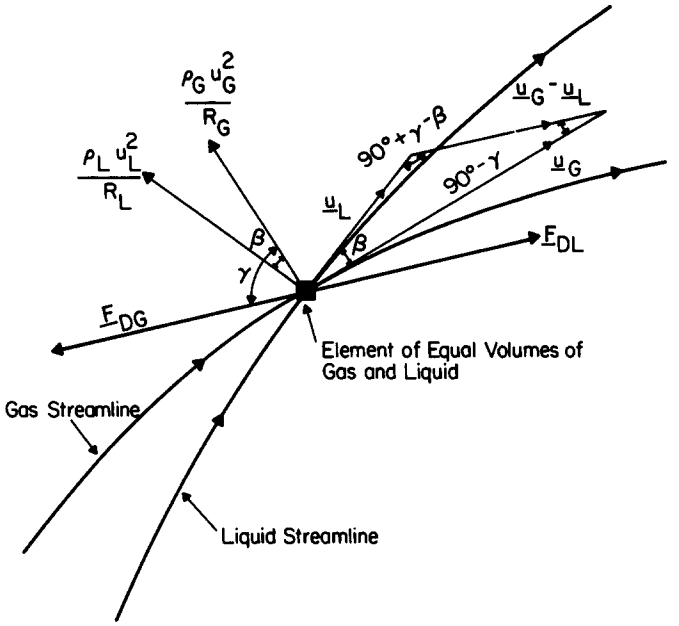

Figure 9. Balance of forces.

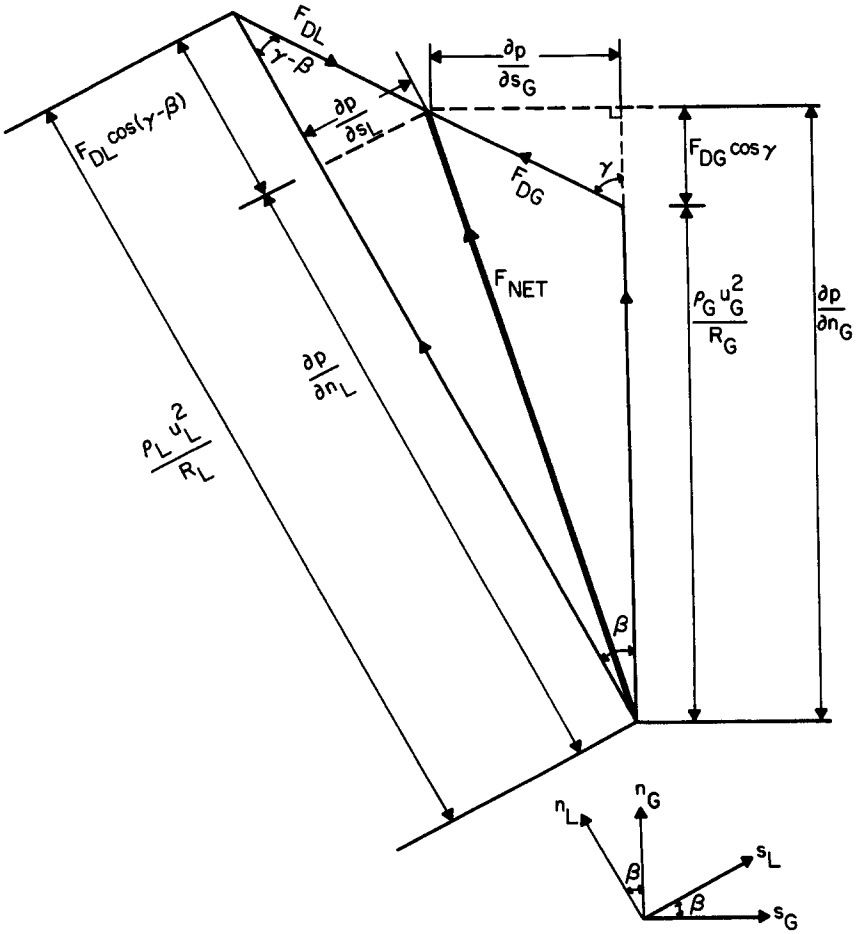

Figure 10. Force vector diagram.

Another important relation can be derived by applying the "sine rule" to the velocity triangle in figure 9:

$$\frac{u_G}{\sin(90^\circ + \gamma - \beta)} = \frac{u_L}{\sin(90^\circ - \gamma)}.$$

Thus,

$$S \triangleq \frac{u_G}{u_L} = \frac{\cos(\gamma - \beta)}{\cos\gamma}. \qquad [17]$$

Equations [16] and [17] are very simple algebraic relations which are a result of a number of simplifying assumptions. Nevertheless, it should be noted that in order to make computations with [16] and [17] we must know the shape of the streamlines. Unfortunately, the actual shapes can only be determined numerically. As an approximation we can assume that the following expression is valid for the gas and liquid dividing streamling in a T-junction:

$$\frac{y}{\delta_k} = 1 - \left(1 - \frac{\eta}{D_3}\right)^{m_k} \quad (k = \text{G or L}). \qquad [18]$$

Equation [18] satisfies the following boundary conditions:

$$y = 0 \quad \text{at} \quad \eta = 0,$$
$$y = \delta_k \quad \text{at} \quad \eta = D_3,$$
$$\frac{dy}{d\eta} = 0 \quad \text{at} \quad \eta = D_3 \quad (m_k > 1).$$

It can also be noted that the streamlines approach straight lines with large radius of curvature, R_k, as $m_k \to 1$. This is expected to be the case for low extraction rates through the side branch (i.e. low δ_k). On the other hand, as $m_k \to 2$, the streamlines become parabolic, with relatively small radius of curvature. Numerical evaluations of the modified Euler s and n equations have indicated that this corresponds to high extraction rates where $\delta_k \to D_1$. Hence, the empirical parameter m_k is assumed to satisfy

$$m_k = 1 \quad \text{at} \quad \delta_k = 0,$$

and

$$m_k = 2 \quad \text{at} \quad \delta_k = D_1.$$

From [18], we have

$$\left.\frac{dy}{d\eta}\right|_{\eta=0} = m_k\left(\frac{\delta_k}{D_1}\right)\frac{D_1}{D_3}$$

hence, the angle β between the dividing streamlines at the impact point ($\eta = 0$) is given by

$$\beta = \tan^{-1}\left(m_G \frac{\delta_G}{D_1}\frac{D_1}{D_3}\right) - \tan^{-1}\left(m_L \frac{\delta_L}{D_1}\frac{D_1}{D_3}\right). \qquad [19]$$

Moreover, from simple analytical geometry considerations, [18] implies the following formulation for the radius of curvature of the dividing streamline of phase k at the impact point ($\eta = 0$):

$$\frac{R_k}{D_3} = \frac{\left[1 + \left(\left.\frac{dy}{d\eta}\right|_{\eta=0}\right)^2\right]^{3/2}}{\left|\left.\frac{d^2y}{d\eta^2}\right|_{\eta=0}\right|} = \frac{\left[1 + \left(m_k \frac{\delta_k}{D_1}\frac{D_1}{D_3}\right)^2\right]^{3/2}}{m_k(m_k - 1)\frac{\delta_k}{D_1}\frac{D_1}{D_3}}. \qquad [20]$$

We note that the minimum radius of curvature occurs when $m_k = 2$ and $\delta_k/D_1 = 1$. For this case, [20] yields

$$\frac{R_k}{D_3} = \frac{\left[1 + \left(2\frac{D_1}{D_3}\right)^2\right]^{3/2}}{2\left(\frac{D_1}{D_3}\right)}. \qquad [21a]$$

For our data, $D_1 = D_3$, thus [21a] becomes

$$\left.\frac{R_k}{D_3}\right|_{\min} = 5.5902. \qquad [21b]$$

Rather than using [20] and correlating m_k from the data it was found to be more convenient to correlate $n_k = n_k(\delta_k/D_1)$, where

$$\frac{R_k}{D_3} \simeq \frac{\left.\frac{R_k}{D_3}\right|_{\min}}{\left(\frac{\delta_k}{D_1}\right)^{n_k}}. \qquad [22]$$

It should be noted that this phase separation model is valid for any inlet flow regime, provided that we know the lateral distribution of the phases.

4.2.3. Separated flows

For the special case of separated flow regimes, such as stratified and annular flows, it has been found that the influence of the interfacial drag force, F_D, is relatively small and can be neglected. Moreover, the vapor and liquid may only interact at or near the stagnation point and thus the use of F_D is not appropriate. Hence, if we neglect this term we obtain from figure 10 that the centrifugal force of the gas is equal to that of the liquid:

$$\frac{\rho_G u_G^2}{R_G} = \frac{\rho_L u_L^2}{R_L}. \qquad [23]$$

Thus, [22] and [23] yield

$$\frac{R_G}{R_L} = \left(\frac{\rho_G}{\rho_L}\right)\left(\frac{u_G}{u_L}\right)^2 = \frac{\left(\frac{\delta_L}{D_1}\right)^{n_L}}{\left(\frac{\delta_G}{D_1}\right)^{n_G}}; \qquad [24a]$$

also, we can write the identity

$$\frac{R_G}{D_3} = \left(\frac{R_L}{D_3}\right)\left(\frac{R_G}{R_L}\right) = \frac{\left(\frac{R_L}{D_3}\right)\left(\frac{\delta_L}{D_1}\right)^{n_L}}{\left(\frac{\delta_G}{D_1}\right)^{n_G}}. \qquad [24b]$$

Equations [16] and [17] are thus not needed for the analysis of separated flows. That is, once we get the value of R_L/D_3, R_G/D_3 can be calculated using [24b].

4.3. Extension of the Phase Separation Model to Other Branching Conduit Configurations

4.3.1. Introduction

The objective here is to extend the ideas just discussed for dividing flows in T-junctions to dividing flows in Y-junctions. It is felt that the physical basis of our previous model, in which the centrifugal and drag forces were identified as the dominant forces controlling phase distribution in the junction, is also appropriate for dividing Y-junctions of various angles (θ). While the force balance equations developed earlier for dividing flows in a T-junction are applicable without modification to dividing flow in a Y-junction, the degree of phase separation will vary due to the influence of angle θ on the curvature of the streamline.

Before proceding with the analysis it is interesting to consider the expected influence of the side branch angle, θ, on phase distribution. For $D_1 = D_3$ (our case) and small values of θ, where $\theta = 0°$ is a straight conduit, Δp_{13_j} is expected to be small. Consequently, the deviation of the dividing streamlines from straight lines should also be small and the deviation from an equal phase split should be small. In the limit, as $\theta \to 0°$ we expect, $\Delta p_{13_j} = 0$ and $x_1 = x_2 = x_3$.

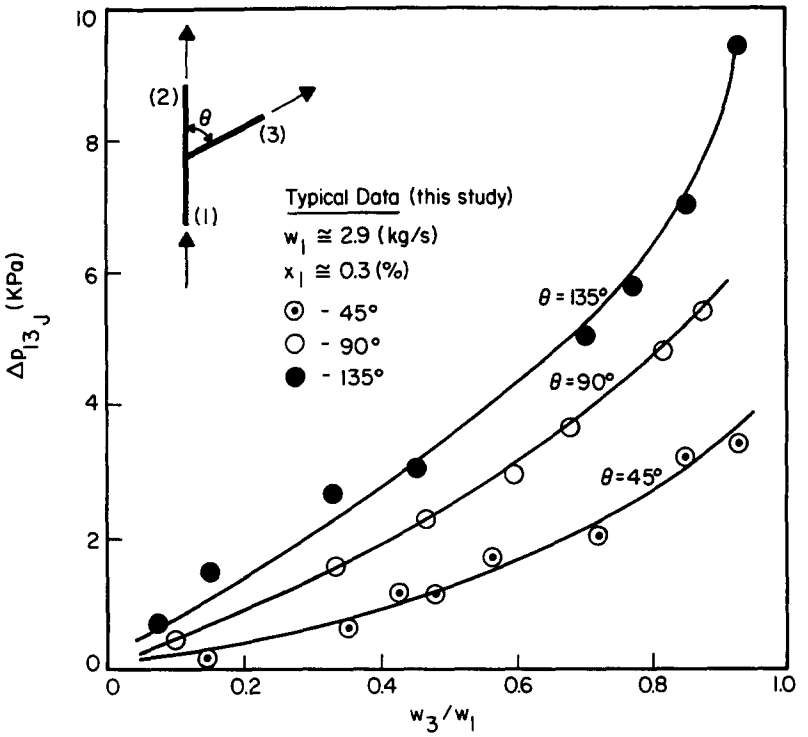

Figure 11. Δp_{13_J} vs w_3/w_1 for dividing flows.

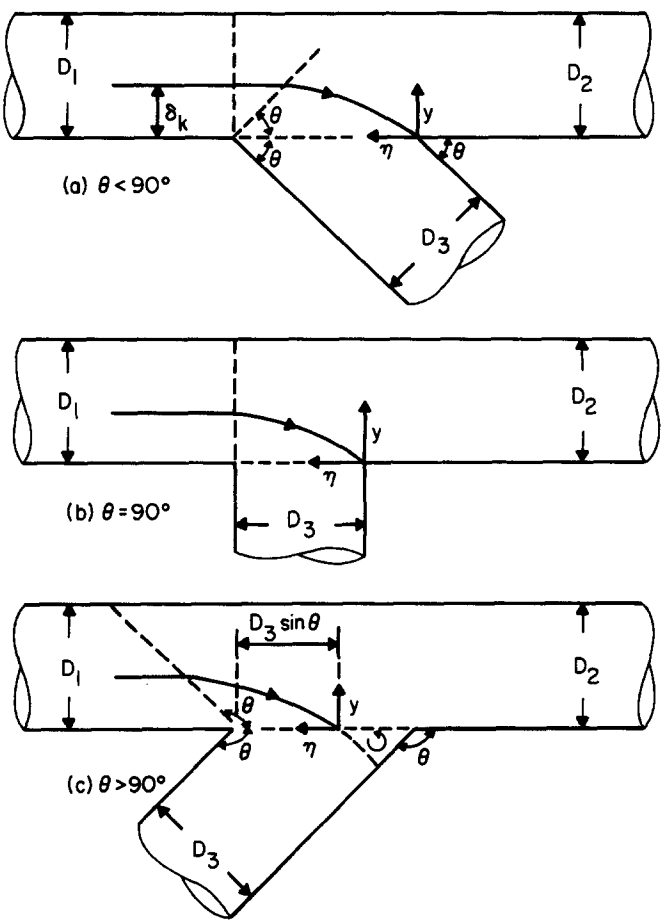

Figure 12. Dividing streamline in each configuration for dividing flows.

On the other hand as shown in figure 11, as θ increases Δp_{13_j} also increases, which implies a decrease in the radius of curvature of the dividing streamlines and a significant departure from an equal phase split. As we approach $\theta = 180°$, the phase separation should approach the condition $x_3/x_1 = 1/x_1$ for $w_3/w_1 < x_1$, and $x_3/x_1 = w_1/w_3$ for $w_3/w_1 \geqslant x_1$. Based on the above discussion, as well as actual measurements of the pressure distribution and visual observations of the flow in the junction, we propose that the form of the dividing streamlines are as shown in figure 12. Due to the measured influence of θ on Δp_{13_j} and observations of the flow, it is reasonable to expect that the dividing streamlines begin turning towards the branch sooner as θ increases. Also for $\theta > 90°$, visual observations indicate a stagnant zone with eddies, as shown in figures 5 and 12.

4.3.2. Diverging streamlines for the case where $0° < \theta \leqslant 90°$

For cases where the angle of divergence is small, we propose the following expression for dividing streamlines:

$$\frac{y}{\delta_k} = 1 - \left(1 - \frac{\eta \sin\theta}{D_3 - \delta_k \cos\theta}\right)^{m_k}. \qquad [25]$$

Equation [25] satisfies the following necessary requirements:

$$y = 0 \quad \text{at} \quad \eta = 0, \qquad [26a]$$

$$y = \delta_k \quad \text{at} \quad \eta = \frac{D_3}{\sin\theta} - \frac{\delta_k}{\tan\theta}, \qquad [26b]$$

$$\left.\frac{dy}{d\eta}\right|_{\eta = \left(\frac{D_3}{\sin\theta}\right) - \left(\frac{\delta_k}{\tan\theta}\right)} = 0 \quad (m_k > 1). \qquad [26c]$$

From [25], we can obtain

$$\left.\frac{dy}{d\eta}\right|_{\eta=0} = m_k \frac{\sin\theta}{\left(\dfrac{\dfrac{D_3}{D_1}}{\dfrac{\delta_k}{D_1}} - \cos\theta\right)}$$

and

$$D_3 \left.\frac{d^2y}{d\eta^2}\right|_{\eta=0} = -m_k(m_k - 1)\frac{\dfrac{D_3}{D_1}}{\dfrac{\delta_k}{D_1}}\left(\frac{\sin\theta}{\dfrac{\dfrac{D_3}{D_1}}{\dfrac{\delta_k}{D_1}} - \cos\theta}\right)^2.$$

Consequently, the radius of curvature is given by

$$\frac{R_k}{D_3} = \frac{\left[1 + \left(\dfrac{m_k \sin\theta}{\dfrac{\dfrac{D_3}{D_1}}{\dfrac{\delta_k}{D_1}} - \cos\theta}\right)^2\right]^{3/2}}{\dfrac{\dfrac{D_3}{D_1}}{\dfrac{\delta_k}{D_1}}\left(\dfrac{\sin\theta}{\dfrac{\dfrac{D_3}{D_1}}{\dfrac{\delta_k}{D_1}} - \cos\theta}\right)^2 m_k(m_k - 1)} \qquad [27]$$

and the angle of intersection of the streamlines by

$$\beta = \tan^{-1}\left[\frac{m_G \sin\theta}{\dfrac{D_3}{D_1} - \dfrac{\delta_G}{D_1} - \cos\theta}\right] - \tan^{-1}\left[\frac{m_L \sin\theta}{\dfrac{D_3}{D_1} - \dfrac{\delta_L}{D_1} - \cos\theta}\right]. \quad [28]$$

Notice that, in the limit as $\theta \to 0$, $R_k/D_3 \to \infty$ for all values of δ_k/D_1. For $0° < \theta \leqslant 90°$, we will follow the assumption adopted earlier for the case of a T-junction that m_k ranges from 1 at $\delta_k/D_1 = 0$ to 2 at $\delta_k/D_1 = 1$. Hence, the minimum value of R_k/D_3 (corresponding to $\delta_k/D_1 = 1$ and $m_k = 2$) can be written as

$$\left.\frac{R_k}{D_3}\right|_{\min} = \frac{\left[1 + \left(\dfrac{2\sin\theta}{\dfrac{D_3}{D_1} - \cos\theta}\right)^2\right]^{3/2}}{\dfrac{2D_3}{D_1}\left(\dfrac{\sin\theta}{\dfrac{D_3}{D_1} - \cos\theta}\right)^2}. \quad [29]$$

Note that for $\theta = 90°$ and $D_3/D_1 = 1$, $R_k/D_3|_{\min} = 5.5902$, as before.

Over the range, $0 < \delta_k/D_1 \leqslant 1$, the radius of curvature can be calculated from the same empirical relation that was used for the T-junction:

$$\frac{R_k}{D_3} = \frac{\left.\dfrac{R_k}{D_3}\right|_{\min}}{\left(\dfrac{\delta_k}{D_1}\right)^{n_k}}, \quad [30]$$

where n_k may now be an empirical function of both δ_k/D_1 and θ.

4.3.3. Diverging streamlines for the case where $90° \leqslant \theta < 180°$

A similar set of relations can be written as before. The expression assumed for the dividing streamlines is given by

$$\frac{y}{\delta_k} = 1 - \left(1 - \frac{\eta \sin\theta}{D_3 \sin^2\theta - \delta_k \cos\theta}\right)^{m_k} \quad [31]$$

which results in the following relationships for the radius of curvature, R_k, and angle, β, between the two streamlines:

$$\frac{R_k}{D_3} = \frac{\left[1 + \left(\dfrac{m_k \sin\theta}{\dfrac{D_3}{D_1} - \dfrac{\delta_k}{D_1}\sin^2\theta - \cos\theta}\right)^2\right]^{3/2}}{\dfrac{D_3}{D_1}\dfrac{\delta_k}{D_1}\left(\dfrac{\sin\theta}{\dfrac{D_3}{D_1} - \dfrac{\delta_k}{D_1}\sin^2\theta - \cos\theta}\right)^2 m_k(m_k - 1)} \quad [32]$$

and

$$\beta = \tan^{-1}\left[\frac{m_G \sin\theta}{\frac{D_3}{D_1}\sin^2\theta - \cos\theta}\right] - \tan^{-1}\left[\frac{m_L \sin\theta}{\frac{D_3}{D_1}\sin^2\theta - \cos\theta}\right]. \quad [33]$$

Naturally, [30] is still valid for this case and the following expression is valid for the minimum radius of curvature:

$$\left.\frac{R_k}{D_3}\right|_{min} = \frac{\left[1 + \left(\frac{2\sin\theta}{\frac{D_3}{D_1}\sin^2\theta - \cos\theta}\right)^2\right]^{3/2}}{\frac{2D_3}{D_1}\left(\frac{\sin\theta}{\frac{D_3}{D_1}\sin^2\theta - \cos\theta}\right)^2}. \quad [34]$$

An empirical function for $n_k(\delta_k/D_1, \theta)$ which was found to give good agreement between the analytical predictions and the data for dividing T-junctions is

$$n_k\left(\theta = 90°, \frac{\delta_k}{D_1}\right) = 5 + 20\exp\left[-53.0\left(\frac{\delta_k}{D_1}\right)\right]. \quad [35]$$

It is interesting to note that for larger extraction rates where $\delta_k \to D_1$, $n_k(\theta = 90°, \delta_k/D_1 \simeq 1) \cong 5$. In order to account for the observed increase radius of curvature for $\theta < 90°$, and the decrease in the radius of curvature for $\theta > 90°$, it was found that for dividing Y-junctions one can approximate the branch angle dependence by

$$n_k\left(\theta, \frac{\delta_k}{D_1}\right) = \frac{n_k\left(\theta = 90°, \frac{\delta_k}{D_1}\right)}{\sqrt{\sin\theta}} \quad \text{for} \quad 0° < \theta \leqslant 90°, \quad [36a]$$

$$n_k\left(\theta, \frac{\delta_k}{D_1}\right) = n_k\left(\theta = 90°, \frac{\delta_k}{D_1}\right)\sin\theta \quad \text{for} \quad 180° > \theta \geqslant 90°. \quad [36b]$$

In addition to the above relations, the two expressions developed earlier from the force balance, [16] and [17], remain unchanged and valid. Finally, it should also be noted that the phase separation model for dividing flows in both Y- and T-junctions is valid for all flow regimes, however, one must know what the flow regime is and how the phases are distributed in the inlet branch to use the model. Once the nonlinear algebraic equations comprising the model are solved (iteratively) to yield δ_G and δ_L, and thus, as can be seen in figure 8, the "zone of influence", and the inlet distribution of each phase is known, the flow rates w_{L_3} and w_{G_3} can be easily calculated. Hence the dividing streamline model yields the "fifth equation" that we need for closure.

4.4 Comparisons with Data

Most previous researchers have studied phase separation in dividing flows in T-junctions. Moreover, the whole mass extraction rate (w_3/w_1) range has not previously been investigated. Some researchers investigated only high extraction rates resulting in almost complete phase separation [i.e. $x_3/x_1 = (w_3/w_1)^{-1}$]. Other data had very narrow ranges of mass extraction. Fortunately our data has filled in many of these blanks. Tables 1–3 present our T- and Y-junction data for air/water dividing flows.

For the proper assessment of our phase separation model representative data was selected and grouped by flow regime. In particular, we chose three flow regimes to analyze:

(A) *Stratified flow*

Hwang (1986) air/water data
Saba & Lahey (1984) air/water data
Seeger (1985) air/water and steam/water data

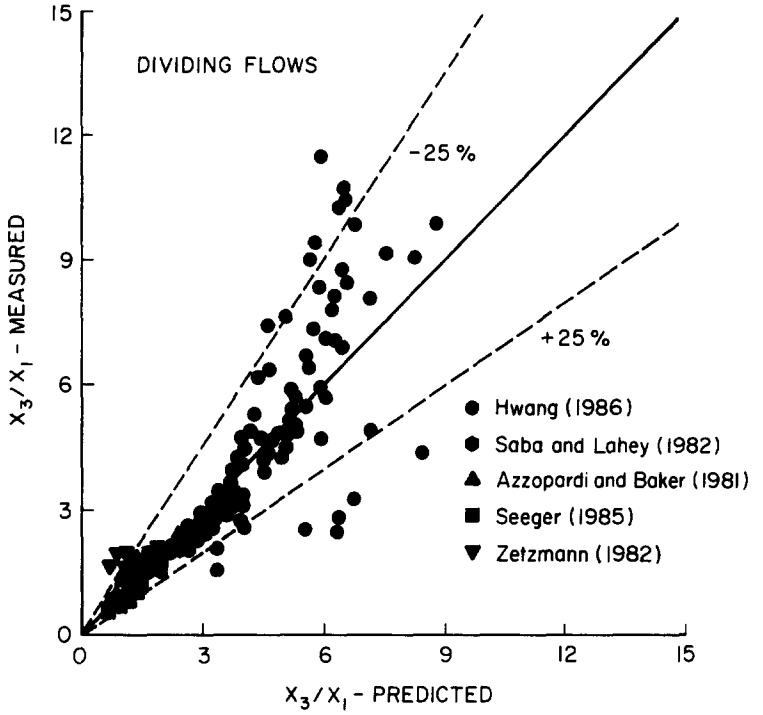

Figure 13. x_3/x_1 measurement vs predicted (dividing flows).

Table 1. Dividing T-junction data

w_1(kg/s)	x_1(%)	$\frac{w_3}{w_1}$	$\frac{x_3}{x_1}$
1.512	0.1451	0.0989	6.459
1.540	0.1733	0.1569	5.151
1.521	0.1540	0.1940	4.422
1.540	0.1569	0.3247	2.531
1.513	0.2428	0.0196	1.427
1.513	0.2441	0.1081	7.108
1.536	0.2158	0.1576	5.106
1.546	0.2657	0.1755	4.812
1.513	0.2445	0.1903	4.412
1.541	0.2156	0.3249	2.508
1.534	0.3497	0.1074	6.896
1.520	0.3486	0.3066	3.159
1.524	0.3475	0.3823	2.603
2.262	0.2279	0.2149	4.079
2.294	0.1540	0.2142	3.891
2.283	0.1548	0.0975	5.470
2.293	0.1096	0.0960	5.885
2.296	0.2313	0.1008	8.324
2.241	0.3152	0.1047	7.766
2.218	0.3142	0.0418	4.369
2.227	0.2003	0.0412	1.522
2.326	0.3373	0.2594	2.229
2.386	0.3203	0.2926	3.435
3.148	0.1054	0.2491	3.119
3.127	0.1471	0.2512	3.352
3.198	0.1232	0.3138	2.558
3.198	0.1286	0.1931	3.956
3.046	0.1349	0.1030	4.496
2.996	0.1372	0.0217	1.557
3.049	0.2230	0.0218	1.233
3.129	0.2228	0.2114	4.019
2.865	0.3387	0.3125	3.138
3.132	0.3146	0.2108	3.967
2.905	0.3340	0.0174	0.890

(B) *Bubbly/dispersed flow*
Zetzmann (1982) air/water data
Seeger (1985) air/water data
(C) *Annular flow*
Azzopardi & Baker (1981) air/water data
Zetzmann (1982) air/water data
Seeger (1985) air/water and steam/water data.

As can be seen in figure 13, the mean of the ratio, $(x_3/x_{1,\text{measured}})/(x_3/x_{1,\text{predicted}})$, was 1.02 with a standard deviation of 0.103. Moreover, our dividing streamline model predicted more than 97% of the available world's data for dividing flows to within $\pm 25\%$.

Finally, it should be noted in figure 13 that some of the data taken in this study (Hwang 1986) exhibits the greatest deviation from the model predictions. These data were all taken for low extraction rates (w_3/w_1). As can be seen in figure 6, this is where the slope of the x_3/x_1 vs w_3/w_1 curves is very steep. As consequence any deviation between measurement and prediction is greatly

Table 2. Diverging Y-junction (45°) data for two-phase flow

Low mass flow rates			
w_1(kg/s)	x_1(%)	$\frac{w_3}{w_1}$	$\frac{x_3}{x_1}$
1.575	0.2001	0.0480	0.075
1.590	0.1978	0.0940	0.117
1.600	0.1964	0.2105	4.186
1.600	0.1981	0.2972	2.926
1.600	0.1964	0.3839	2.363
1.604	0.1959	0.5134	1.793
1.594	0.1985	0.5937	1.628
1.594	0.1971	0.7521	1.241
1.600	0.1964	0.8554	1.092
1.583	0.1986	0.9595	0.993
1.602	0.3062	0.0689	0.033
1.602	0.3071	0.1083	0.204
1.601	0.2991	0.1994	4.453
1.601	0.2988	0.3055	2.815
1.601	0.2988	0.3745	1.318
1.602	0.3019	0.5194	1.884
1.597	0.2987	0.6093	1.596
1.593	0.3013	0.7394	1.312
1.585	0.3019	0.7967	1.251
1.573	0.3053	0.8995	1.077
1.583	0.4086	0.0697	0.025
1.595	0.4057	0.1011	0.069
1.599	0.4047	0.2032	4.829
1.603	0.4037	0.3089	3.178
1.606	0.4031	0.4073	2.420
1.599	0.4044	0.5347	1.848
1.606	0.4031	0.6346	1.560
1.599	0.4047	0.6831	1.453
1.589	0.4069	0.8225	1.176
1.578	0.4100	0.8732	1.119
2.362	0.2014	0.0627	0.042
2.329	0.2049	0.1148	4.754
2.351	0.2030	0.2222	2.189
2.362	0.2014	0.2993	2.911
2.306	0.2036	0.4758	2.063
2.415	0.1975	0.5061	1.966
2.295	0.2039	0.5479	1.703
2.295	0.2039	0.7393	1.298
2.306	0.2029	0.8129	1.159
2.250	0.2087	0.9244	1.059
2.275	0.2964	0.0582	0.064
2.308	0.2918	0.1256	7.409
2.314	0.2911	0.2348	3.949
2.336	0.2883	0.3317	2.889
2.320	0.2906	0.4235	2.287

continued

Table 2—*continued*

Low mass flow rates			
w_1(kg/s)	x_1(%)	$\frac{w_3}{w_1}$	$\frac{x_3}{x_1}$
2.331	0.2890	0.4986	1.967
2.308	0.2918	0.5944	1.679
2.297	0.2937	0.7269	1.364
2.280	0.2959	0.7981	1.245
2.252	0.2996	0.9286	1.060
2.255	0.4182	0.0837	7.320
2.266	0.4161	0.1201	7.619
2.266	0.4161	0.1864	4.898
2.277	0.4140	0.2681	3.496
2.322	0.4074	0.4135	2.355
2.322	0.4064	0.4902	1.969
2.289	0.4120	0.5724	1.705
2.260	0.4171	0.7404	1.484
2.255	0.4182	0.8610	1.273
2.243	0.4203	0.8901	1.119
2.811	0.2130	0.0687	6.369
2.817	0.2119	0.1048	6.189
2.833	0.2121	0.1724	4.748
2.861	0.2100	0.3298	2.648
2.901	0.2104	0.4200	2.200
2.969	0.2029	0.4841	1.925
2.883	0.2086	0.6257	1.517
2.868	0.2095	0.7624	1.253
2.824	0.2121	0.8527	1.135
2.808	0.2130	0.8895	1.054
2.810	0.2925	0.0633	5.043
2.827	0.2940	0.1487	5.315
2.851	0.2901	0.2051	4.258
2.878	0.2918	0.3418	2.634
2.903	0.2900	0.4205	2.228
2.913	0.2907	0.4747	1.995
2.886	0.2930	0.5612	1.710
2.851	0.2941	0.7226	1.365
2.813	0.2913	0.8574	1.149
2.799	0.2928	0.9337	1.055
2.808	0.4020	0.0664	4.717
2.813	0.3944	0.0852	4.913
2.838	0.4054	0.2069	4.129
2.854	0.4078	0.2908	3.103
2.867	0.4136	0.4383	2.175
2.873	0.4050	0.5115	1.916
2.873	0.4019	0.5918	1.673
2.838	0.4060	0.6760	1.475
2.811	0.4059	0.8130	1.231
2.796	0.4056	0.9046	1.042

Table 3. Diverging Y-junction (135°) data for two-phase flow

Low mass flow rates			
w_1(kg/s)	x_1(%)	$\frac{w_3}{w_1}$	$\frac{x_3}{x_1}$
1.567	0.2004	0.0403	0.189
1.578	0.1991	0.0823	7.070
1.575	0.1993	0.1196	6.387
1.575	0.1993	0.1816	4.206
1.588	0.1978	0.2795	2.876
1.583	0.1983	0.3897	2.039
1.579	0.2001	0.5172	1.810
1.579	0.1988	0.5976	1.594
1.562	0.2022	0.7372	1.229
1.562	0.2052	0.7938	1.125
1.549	0.2071	0.8979	1.003
1.573	0.3165	0.0443	1.476
1.542	0.3215	0.0776	8.096
1.564	0.3191	0.0952	8.395
1.560	0.3209	0.1745	4.928
1.568	0.3119	0.3521	2.282
1.568	0.3119	0.5653	1.901
1.568	0.3128	0.6013	1.667
1.573	0.3113	0.7284	1.371
1.565	0.3128	0.7734	1.249
1.560	0.3136	0.9123	1.073
1.557	0.4066	0.0406	0.432
1.550	0.4108	0.0655	9.031
1.521	0.4072	0.1193	8.097
1.521	0.4072	0.1773	5.413
1.534	0.3939	0.2736	3.597
1.544	0.4004	0.4028	2.425
1.535	0.4017	0.5755	1.714
1.525	0.4056	0.6344	1.556
1.525	0.4056	0.7183	1.380
1.530	0.4051	0.8439	1.168
1.525	0.4094	0.9132	1.084
2.323	0.2076	0.0393	2.816
2.351	0.2061	0.0946	9.418
2.378	0.2060	0.2112	4.173
2.394	0.2022	0.3020	3.106
2.405	0.2017	0.3537	2.492
2.416	0.2021	0.4183	2.036
2.284	0.2143	0.4993	1.942
2.378	0.2059	0.5625	1.721
2.426	0.1961	0.6891	1.522
2.389	0.1989	0.8074	1.292
2.351	0.2001	0.9640	1.001
2.358	0.2856	0.0453	9.140
2.353	0.2860	0.0806	10.430
2.407	0.2793	0.1883	4.498

continued

Table 3—*continued*

Low mass flow rates			
w_1(kg/s)	x_1(%)	$\frac{w_3}{w_1}$	$\frac{x_3}{x_1}$
2.407	0.2791	0.2861	3.295
2.407	0.2797	0.3744	2.596
2.407	0.2813	0.4815	2.026
2.364	0.2860	0.6735	1.452
2.353	0.2857	0.7207	1.377
2.218	0.3040	0.8175	1.194
2.159	0.3109	0.9893	1.000
2.366	0.3914	0.0443	9.889
2.377	0.3896	0.0641	13.490
2.377	0.3879	0.1023	8.773
2.436	0.3789	0.1635	5.749
2.451	0.3788	0.3344	2.923
2.461	0.3772	0.3740	2.622
2.409	0.3853	0.5305	1.822
2.388	0.3888	0.6823	1.470
2.355	0.3915	0.7520	1.339
2.266	0.4083	0.7757	1.279
2.808	0.2128	0.0339	2.524
2.828	0.2076	0.0635	11.490
2.833	0.2069	0.0897	8.993
2.868	0.2068	0.1997	4.283
2.932	0.2021	0.3347	2.715
2.983	0.2020	0.4874	1.956
2.901	0.2040	0.6100	1.585
2.868	0.2074	0.7373	1.309
2.828	0.2078	0.8254	1.219
2.807	0.2135	0.8977	1.054
2.794	0.2934	0.0362	4.901
2.808	0.2952	0.0712	10.710
2.812	0.2929	0.0781	10.250
2.831	0.2941	0.1791	4.864
2.851	0.2923	0.3205	2.902
2.894	0.2902	0.4540	2.125
2.867	0.2933	0.5034	1.934
2.818	0.2936	0.7827	1.250
2.808	0.2919	0.8233	1.214
2.788	0.2887	0.9337	1.068
2.798	0.3796	0.0341	2.112
2.816	0.3877	0.0814	9.848
2.833	0.3830	0.2158	4.146
2.853	0.3818	0.3181	2.931
2.906	0.3771	0.4024	2.354
2.906	0.3741	0.4635	2.082
2.853	0.3797	0.6475	1.498
2.808	0.3784	0.7941	1.237
2.802	0.3763	0.8660	1.170

amplified. The large apparent scatter seen in figure 13 is due to this amplification of error. Nevertheless, our model does a good job for a wide range of data involving many different flow regimes, conduit configurations and operating conditions (including high-pressure steam/water).

5. CONCLUSIONS

A full range of air/water phase separation data in horizontal Y- and T-junctions has been presented. These data give us valuable new information on the effect of branch angle (θ) and phase separation phenomena at low mass extraction rates.

An analytical model for phase separation in branching conduits was developed. This model was based on a dividing streamline analysis and assumes that the so-called "zone of influence" is determined by the initial position of the dividing streamlines in the inlet branch. This phenomenological model is applicable to all flow regimes for dividing flows in both Y- and T-junctions.

However, in order to perform analysis one needs to know what the inlet flow regime is and how the phases are distributed in the inlet branch.

It should be noted that the phase separation model presented herein is intended for applications in which the side branch is the same size, or nearly the same size, as the inlet duct and the run. For cases in which there is a much smaller diameter side branch (or break), another analytical approach may be necessary. In particular, for small-break-loss-of-coolant-accidents (SBLOCA) in nuclear reactors, the two-phase mixture may be stratified and can be discharged through an opening which is either significantly above or below the free surface. For such cases, consideration of the onset of liquid carryover or vapor pull-through is necessary. Fortunately, sufficiently accurate data and models appear to exist for such cases (Zuber 1981; Crowley & Rothe 1981; Reimann & Khan 1984; Smoglie *et al.* 1986; Anderson & Owca 1985). It is recommended at this time that the model of Smoglie *et al.* (1986) be used in conjunction with the model presented herein for SBLOCA analysis.

Acknowledgements—The authors wish to acknowledge the financial support given this work by the National Science Foundation and the Natural Sciences and Engineering Research Council of Canada.

NOMENCLATURE

D = Diameter, m
f = Friction factor
F = Force, N
K_i = Loss coefficient at location i
g = Gravity, m/s^2
G_i = Mass flux at position i, kg/m^2 s
L_i = Length of branch i
p = Pressure, N/m^2
R = Radius of curvature, m
S = Slip ratio $\left(\frac{u_G}{u_L}\right)$
u_k = Velocity of phase k, m/s
w_i = Mass flow rate at position i, kg/s
x = flow quality

Greek

β, γ = Angles
δ_k = Position of the dividing streamline of phase k, m
Δp_{ij} = Static pressure change from position i to position j, N/m^2
η = Spatial coordinate defined implicitly in figure 8
ρ = Density, kg/m^3
ρ' = Momentum density, kg/m^3 (Lahey & Moody 1977)
ρ''' = Energy density, kg/m^3 (Lahey & Moody 1977)
ρ_H = Homogeneous density, kg/m^3 (Lahey & Moody 1977)
ϕ^2_{L0} = Two-phase friction multiplier
Φ = Two-phase local loss multiplier
θ_i = Angle of inclination of branch i from the horizontal

Subscripts

1 = Inlet
2 = Run
3 = Branch
J = Junction
G = Gas phase
L = Liquid phase
H = Hydraulic

REFERENCES

ANDERSON, J. L. & OWCA, W. A. 1985 Data report for the TPFL tee/critical flow experiments. Report NUREG/CR-4164, EGG-2377.

AZZOPARDI, B. J. & BAKER, S. R. 1981 Two-phase flow in a 'T' junction. The effect of flow pattern in vertical upflow. Report AERE-R 10174.

AZZOPARDI, B. J. & WHALLEY, P. B. 1982 The effect of flow patterns on two-phase flow in a 'T' junction. *Int. J. Multiphase Flow* **8,** 491–507.

COLLIER, J. 1975 Single-phase and two-phase flow behavior in primary circuit components. Presented at *Symp. on Two-phase flow and Heat Transfer in Water-cooled Nuclear Reactors*, Dartmouth College, Hanover, N.H.

CROWLEY, C. J. & ROTHE, P. H. 1981 Flow visualization and break mass flow measurements in small break separate effects experiments. In *Proc. ANS Specialist Mtg on Small Break Loss of Coolant Accident Analysis in LWRs*, Monterey, Calif.

HENRY, J. A. R. 1981 Dividing annular flow in a horizontal tee. *Int. J. Multiphase Flow* **7,** 343–355.

HONAN, T. J. & LAHEY, R. T. JR 1981 The measurement of phase separation in wyes and tees. *Nucl. Engng Des.* **54,** 93–102.

HWANG, S. T. 1986 A study on phase separation phenomena in branching conduits. Ph.D. Thesis, Rensselaer Polytechnic Inst., Troy, N.Y.

HWANG, S. T. & LAHEY, R. T. JR 1988 A study on single and two-phase pressure drop in branching conduits. *Expl therm. Fluid Sci.* **1,** 1–15.

LAHEY, R. T. JR 1986 Current understanding of phase separation mechanisms in branching conduits. *J. nucl. Engng Des.* **95,** 145–161.

LAHEY, R. T. JR & MOODY, F. J. 1977 The thermal-hydraulics of a boiling water nuclear reactor. An ANS monograph. American Nuclear Soc., Hindsdale, Ill.

REIMANN, J. & KAHN, M. 1984 Flow through a small pipe at the bottom of a large pipe with stratified flow. *Nucl. Sci. Engng* **88,** 297–310.

REIMANN, J. & SEEGER, W. 1983 Two-phase pressure drop in a dividing T-junction, the mechanics of gas-liquid flow systems. Presented at *Euromech Colloquium 176*, Villard de Lans, France.

SABA, N. & LAHEY, R. T. JR 1984 Phase separation in branching conduits. *Int. J. Multiphase Flow* **10,** 1–20.

SEEGER, W. 1985 Untersuchungen zum Druckabfall und zur Massenstromum-verteilung von Zweiphasenströmungen in Rechtwinkigen Rohrverzweigungen. Report KfK 3876.

SMOGLIE, C., REIMANN, J. & MULLER, U. 1986 Two-phase flow through small breaks in a horizontal pipe with stratified flow. *Nucl. Engng Des.* **99,** 117–130.

ZETZMANN, K. 1982 Phasenseparation und Druckelufall in Zweiphasig Durchstroemten Vertikalen Rohrabzweigungen. Doctorate Thesis, Univ. of Hanover. F.R.G.

ZUBER, N. 1981 Problems in modeling of small break LOCA. Report NUREG/CR-0724.